5th Intercontinental Geoinformation Days

igd.mersin.edu.tr

Implementation of supervised SID algorithm in preparation of map of geological units

Parviz Zeaiean Firouzabadi [1], Parisa Safarbeyranvand [*1], Ali Hosingholizade [1]

[1]*Kharazmi University, Geography, Remote sensing and GIS, Tehran, Iran*

Keywords
Remote sensing
UAV
Photogrammetry
DEM
SID

Abstract

Using remote sensing technology and satellite data often reduces the expenses and increases the speed and accuracy. Providing the map of geological units has improved so that detection and classification of geological units. In this research, it was done by hyperspectral image, related to Khoramabad zone, Lorestan, and also by applying the SID (Spectral Information Divergence) supervised classification algorithm for detection and separation of geological units. After the necessary pre-processes, the MNF conversion and the PPI algorithm were used for reducing data and extracting the pure pixels on the image. Then extracted for each member by the overlay of pure pixels with geological units and ground data, these pure members were used as input for the mentioned algorithm and the image was classified. Finally, the classification accuracy of this method (66/71) was obtained.

1. Introduction

Preparing a map of geological units, while identifying valuable mineral deposits, creates a suitable and integrated vision of the study area for managers and decision makers (Sousa and Sousa. 2020). In the past, maps of geological units were usually prepared by traditional methods, including visual inspection with laboratory sampling (Lorenz et al. 2021) It is while these days, the use of remote sensing images, especially hyperspectral images, due to the use of many spectral bands and in a very narrow range of the electromagnetic spectrum, reduces costs and increases accuracy and speed (Qasim et al. 2022). On the other hand, the vastness of the regions makes it necessary to use precise and piracy methods that are able to process and extract valuable information from this mass data (Douglas et al. 2022). The use of remote sensing technology as one of the most important tools for collecting information has been the focus of many experts and specialists in various sciences, especially geology, mining, environment, meteorology and agriculture (Schodlok et al. 2022). Compared to multispectral images, hyperspectral images provide data with higher spectral resolution and identify land features more accurately (Stuart et al. 2022). In hyperspectral remote sensing, even the reflection of earth surface phenomena can be measured in very narrow bands with a spectral width of 0.01 micrometers in the spectral range of 0.4 to 2.5 (Johnson et al. 2019). Narrow and wide spectral bands of hyperspectral images provide the possibility of

Geological research and identification of geological units of the region with better results (Ramanaidou et al. 2012). In this research, it has been tried to use the capabilities of remote sensing technology to prepare these maps.

Remote sensing technology images provide efficient data that requires processing on the image to extract the necessary information (Barton et al. 2021). Among the different methods of remote sensing, the classification technique has a special place in the analysis, separation and recognition of different geological units. Image classification is one of the main components of the subject information extraction process, which is done by examining the relationship between the spectral effect and different classes or classifications (Fonteneau et al. 2019). The algorithm used in this research is supervised. Examining the supervised algorithm with full pixels and the results of these algorithms will help us to improve the classification and detection of the desired targets (Johnson et al. 2019). That is, which algorithms are more efficient in preparing maps of geological units. In this research, an attempt has been made to increase

* **Corresponding Author**

(p.zeaiean@gmail.com) ORCID ID 0000-0001-8407-5605
*(pbeyranvandgis@gmail.com) ORCID ID 0000 – 0002 – 7860 – 2621
(a.hosingholizade@ut.ac.ir) ORCID ID 0000 – 0001 – 5286 – 1361

Cite this study

Zeaiean Firouzabadi P, Safarbeyranvand P & Hosingholizade A (2022). Plying to SID supervised algorithm in providing the map of geological units. 5th Intercontinental Geoinformation Days (IGD), 60-63, Netra, India

the accuracy of the created maps by classification and diagnosis based on the obtained spectra, and to identify geological units with the help of Hyperion satellite images and separation.

2. Method

2.1. Study area

The studied area is located in the west of Iran, Lorestan province,
Khorramabad city. Khorramabad is geographically located in the range of 33 degrees, 29 minutes north latitude and 48 degrees, 21 minutes east longitude. Examining the structural-sedimentary situation of the province shows that its different parts have acquired different geological features over time and have been differentiated from each other, therefore according to the tectonic activities and construction style of the different age units or sedimentary basins and the type of sediments related to them Also, the magmatic and metamorphic activities of Lorestan province are highly diverse based on geological and structural units (Noroozi et al. 2015).

2.2. Satellite image of Hyperion sensor EO-1

The image used in this research was taken on September 14, 2019. The coordinates of the center of the zone and image are 31°N3700.09" and 47°E53'19.11". Spectral curve effect correction is one of the necessary corrections for Hyperion data, performed by pushbroom 1 imaging technology, and is present in all Hyperion data. Also, error correction was done by adjusting the average in the luminance space.1. Visible-near infrared

2.3. Band Selection

Among the 242 spectral bands of the Hyperion sensor used in this research, 196 bands are calibrated and unique, and 155 bands were entered into the processing stage by removing the bands that absorb water or have a lot of noise. Table 1 shows the range of acceptable electromagnetic wavelengths for entering the processing stage.

Table 1. Acceptable bands which enter processing

Spectral range	Acceptable bands
VNIR range	8-57 79
SWIR range	83-119 133-164 183-184 188-122

2.4. Minimum Noise Fraction

Transform (MNF) reduces data dimensionality and noise when using hyperspectral data. The MNF transform is considered as a noise reduction transform. It is a linear transformation that is used to determine the original dimensions and volume of the image, separate noise from other information and reduce the degree of processing in the next step. In this conversion, the image is first converted to noise and noise-free, then the noise-free part is considered as the main part and the noise is removed.

2.5. Implementation of the image purity index (PPI)

PPI algorithm is used in hyperspectral images to find pure pixels (final pixels). For this purpose, the ten output bands obtained from the MNF transformation, which are noise-free, are given as input to the PPI algorithm. The output of this algorithm is an image that specifies pure pixels.

2.6. Endmember spectrum extraction and Endmember extraction through pure pixel identification

Many classification algorithms in hyperspectral images need to enter the spectral characteristics of the members (any class or complex that is classified or revealed in the hyperspectral image is called a member) to start processing.

Pure members were extracted from areas where the type of geological unit was identified. With 4 stages of surveying and field surveying and recording the coordinates of geological units using a high-precision GPS device and using the sampled points that corresponded to the pure pixels extracted from the PPI algorithm, the average reference spectrum of the units was extracted from the image itself and this reference spectrum It was used as an input for the classification algorithm (Figure 1).

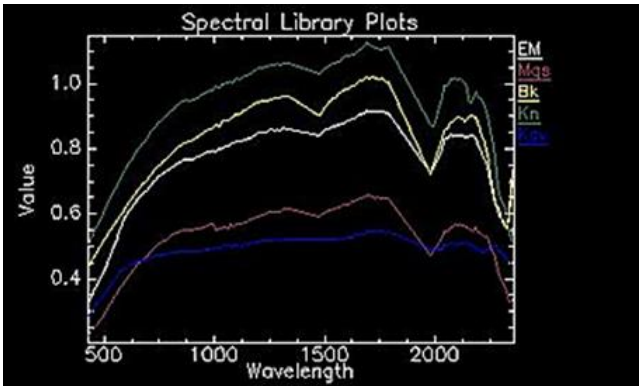

Figure 1. The electromagnetic spectrum extracted from the image related to the geological units of the region

2.7. Spectral Information Divergence

The spectral similarity between two pixels vectors was measured based on the probability distribution difference obtained from their spectral signatures (1).

$$SID = \sum_{l=1}^{L} p_1 \log(p_1 / q_1) + \sum_{l=1}^{L} q_1 \log(q_1 / p_1)$$

$$p_1 = s_{jl} / \sum_{k=1}^{L} s_{lk}$$

$$q_1 = s_{jl} / \sum_{k=1}^{L} s_{jk}$$

Where p1 and q1 are spectral component probability of Si1 and Sj1 of two-pixel vectors of and rj respectively and L is the vector dimension. In the above method, the obtained value should be normal to have a picture in the range of 0 to 1.

Table 2. Stations of study area Guide Sarvkad

Guide	Sarvkad
Casestudy: Khoramabad	Bakhtiari
Used algorithm: SID	Kashkan Asmari –Shahbazan Gachsaran Other Residential area

Table 2 and Figure 2 show the studied station and SID Area map.

3. Results

After processing, the map of the geological formations of the studied area was obtained, divided into seven classes including Sarvak, Bakhtiari, Kashkan, Asmari-Shahbazan, Gachsaran, Residential area and other (Figure 2).

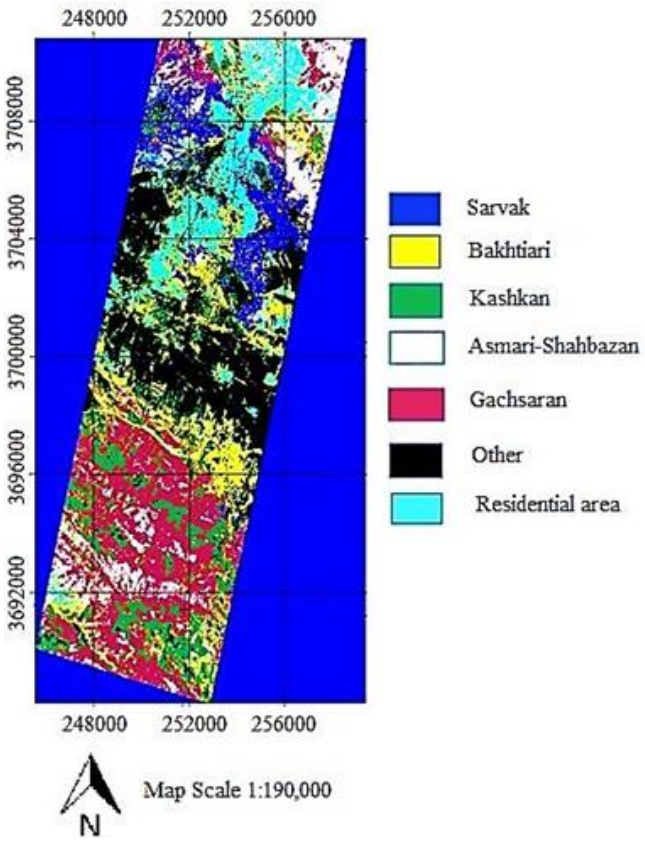

Figure 2. SID Area map

Table 3 shows the area of each of the seven classifications in hectares and Table 4 show Error matrix parameters.

Table 3. Area of geological units using the algorithm

Formation	SID (Hectare)
Sarvak	15334.65
Gachsaran	3696.93
Asmari – Shahbazan	2006.46
Kashkan	2425.59
Bakhtiari	2374.47

Table 4. Error matrix, general accuracy, and kappa coefficients for the results of the SID algorithm

class	Ground data (experimental pixels)						
	residential	Bakhtiari	Kashkan	Asmari	Gachsaran	Sarvak	Full pixels
Not classified	0.42	0.84	0.00	0.00	0.02	0.09	0.07
Sarvak	0.42	0.17	0.19	0.00	0.1	62.97	22.61
Gachsaran	0.42	13.34	4.46	20.92	68.05	4.76	35.98
Asmaran	0.42	19.43	8.33	75.02	28.94	17.60	28.31
Kashkan	0.00	2.53	48.06	0.08	0.87	1.02	1.9
Bakhtiari	1.69	55.57	8.91	3.35	1.96	3.89	4.26
Residential	96.62	3.72	5.04	0.63	0.06	6.02	3.39
others	0	4.39	25	0	0	3.64	3.54
Full pixels	100.00	100.00	100.00	100.00	100.00	100.00	100.00
Total accuracy: 66.71					Kappa coefficient: 0.53		

4. Discussion

The evaluation of the results of this research shows that the comparison of the map of geological units, which was obtained using the SID algorithm, with the maps previously prepared by the Geological Organization of Lorestan province and the Geological Organization of the country, shows the fact that the algorithm SID has a high accuracy with an overall accuracy of 66.71 percent and a kappa coefficient of 0.53 percent. Also, the results show that the SID algorithm is an efficient method for classifying the region based on existing geological units, in the research of preparing geological maps, taking into account the conditions of the region. Due to the high capability of hyperspectral images in the resolution of phenomena, it shows that the identification and separation of geological units using these images is easier and more accurate than other methods such as the use of multi-band images.

5. Conclusion

Preparation of maps of geological units over many years as well as conducting extensive studies and researches has now reached a point where instead of being in the area and doing fieldwork and spending a lot of time and money, with the help of remote sensing and the use of hyperspectral images in It can be done in a short time and with high accuracy. In this research, the SID algorithm was evaluated for the identification of geological units. The results of this study show that SID can help in preparing geological maps for areas where some information on the types of geological units is currently available. According to the results of calculating the area of different formations in the study area as shown in Table (4), Saruk Formation has the largest area calculated in the SID classification method. Therefore, it is suggested that in future research, sensors with a higher spatial resolution than Hyperion (with a pixel size of 30 meters) should be used to identify

valuable geological units in order to produce maps with higher accuracy.

Acknowledgement

The authors of the research are grateful to the General Department of Industries and Mines of Lorestan province and Mr. Alireza Beyranvand.

References

Barton I. F, Gabriel M. J, Lyons-Baral J, Barton M. D, Duplessis L & Roberts C (2021). Extending geometallurgy to the mine scale with hyperspectral imaging: A pilot study using drone-and ground-based scanning. Mining, Metallurgy & Exploration, 38(2), 799-818.

Douglas A, Kereszturi G, Schaefer L. N & Kennedy B (2022). Rock alteration mapping in and around a fossil shallow intrusion at Mt. Ruapehu New Zealand with laboratory and aerial hyperspectral imaging. Journal of Volcanology and Geothermal Research, 107700.

Fonteneau L C, Martini B & Elsenheimer D (2019). Hyperspectral imaging of sedimentary iron ores–beyond borders. ASEG Extended Abstracts, 2019(1), 1-5.

Johnson C. L, Browning D. A & Pendock N. E (2019). Hyperspectral imaging applications to geometallurgy: Utilizing blast hole mineralogy to predict Au-Cu recovery and throughput at the Phoenix mine, Nevada. Economic Geology, 114(8), 1481-1494.

Johnson C. L, Browning D. A & Pendock N. E (2019). Hyperspectral imaging applications to geometallurgy: Utilizing blast hole mineralogy to predict Au-Cu recovery and throughput at the Phoenix mine, Nevada. Economic Geology, 114(8), 1481-1494.

Lorenz S, Ghamisi P, Kirsch M, Jackisch R, Rasti B, & Gloaguen R (2021). Feature extraction for hyperspectral mineral domain mapping: A test of conventional and innovative methods. *Remote Sensing of Environment*, 252, 112129.

Noroozi M, Kakaie R & Jalali S. E (2015). 3D Geometrical-Stochastical modeling of rock mass joint networks: case study of the right bank of Rudbar Lorestan Dam plant. Journal of Geology and Mining Research, 7(1), 1-10.

Qasim M, Khan S. D & Haider R (2022). Integration of multispectral and hyperspectral remote sensing data for lithological mapping in Zhob Ophiolite, Western Pakistan. Arabian Journal of Geosciences, 15(7), 1-19.

Ramanaidou E. R & Wells M. A (2012). Hyperspectral imaging of iron ores. In Proceedings of the 10th International Congress for Applied Mineralogy (ICAM) (pp. 575-580). Springer, Berlin, Heidelberg.

Schodlok M. C, Frei M & Segl K (2022). Implications of new hyperspectral satellites for raw materials exploration. Mineral Economics, 35(3), 495-502.

Sousa, F J, & Sousa D. J (2022). Hyperspectral Reconnaissance: Joint Characterization of the Spectral Mixture Residual Delineates Geologic Unit Boundaries in the White Mountains, CA. *Remote Sensing*, 14(19), 4914.

Stuart M. B, Davies M, Hobbs M. J, Pering T. D, McGonigle A. J & Willmott J. R (2022). High-resolution hyperspectral imaging using low-cost components: Application within environmental monitoring scenarios. Sensors, 22(12), 4652.